

European Journal of Inorganic Chemistry

Catalytic H₂ evolution with CoO, Co(OH)₂ and CoO(OH) NPs generated from a molecular polynuclear Co complex

--Manuscript Draft--

Manuscript Number:	
Article Type:	Full Paper
Corresponding Author:	Antoni Llobet ICIQ Tarragona, SPAIN
Corresponding Author E-Mail:	allobet@iciq.cat
Order of Authors (with Contributor Roles):	Marcos Gil-Sepulcre Carolina Gimbert-Suriñach David Aguila Veronica Velasco Jordi Garcia-Anton Antoni Llobet Guillem Aromi Roger Bofill Xavier Sala
Keywords:	CoO _x Electrocatalysis H ₂ evolution transition metal chemistry
Manuscript Classifications:	Catalysis
Suggested Reviewers:	Sven Rau sven.rau@uni-ulm.de
Opposed Reviewers:	
Abstract:	<p>Electrochemical water reduction by employing first row transition metal nanoparticles (NPs) constitutes a sustainable way for the generation of H₂. We have synthesized Co-based NPs from a molecular CoII/CoIII precursor after its reductive decomposition at -1.86 V vs. NHE in different organic solvents. These NPs are able to electrochemically reduce water at pH 14. SEM, EDX and XPS analyses have allowed the determination of the chemical nature of the as-deposited NPs: CoO when using MeCN as solvent and CoO(OH) when employing either dichloromethane (DCM) or MeOH. After 2h of constant polarization at 10 mA·cm⁻², the electrocatalytic activity of the NPs obtained in MeCN and DCM decreases, whereas for those obtained in MeOH increases. In this solvent, the overpotential is reduced by 215-220 mV and the specific current density is triplicated. Interestingly, during this activation process in MeOH the precursor CoO(OH) NPs are converted into Co(OH)₂. The implications of these results in the context of the current research in the field are also discussed.</p>
Author Comments:	<p>Dear Sirs,</p> <p>Please find attached a contribution from my lab in collaboration with groups from the Univ. of Barcelona and Autonomous of Barcelona.</p> <p>The contribution deals with the formation of CoO_x NP and their application into proton reduction catalysis.</p>

	I hope the work will of interest to you and the readership of EurJIC. Best regards, Toni-
Section/Category:	ICIQ - By Invitation Only
Additional Information:	
Question	Response
Dedication	
Submitted solely to this journal?	Yes
Has there been a previous version?	No

Catalytic H₂ evolution with CoO, Co(OH)₂ and CoO(OH) NPs generated from a molecular polynuclear Co complex

Marcos Gil-Sepulcre,^[a,b] Carolina Gimbert-Suriñach,^[b] David Aguilà,^[c] Verónica Velasco,^[c] Jordi García-Antón,^[a] Antoni Llobet,^[a,b] Guillem Aromí,^{*,[c]} Roger Bofill^{*,[a]} and Xavier Sala^{*,[a]}

Abstract: Electrochemical water reduction by employing first row transition metal nanoparticles (NPs) constitutes a sustainable way for the generation of H₂. We have synthesized Co-based NPs from a molecular Co^I/Co^{III} precursor after its reductive decomposition at -1.86 V vs. NHE in different organic solvents. These NPs are able to electrochemically reduce water at pH 14. SEM, EDX and XPS analyses have allowed the determination of the chemical nature of the as-deposited NPs: CoO when using MeCN as solvent and CoO(OH) when employing either dichloromethane (DCM) or MeOH. After 2h of constant polarization at 10 mA·cm⁻², the electrocatalytic activity of the NPs obtained in MeCN and DCM decreases, whereas for those obtained in MeOH increases. In this solvent, the overpotential is reduced by 215-220 mV and the specific current density is triplicated. Interestingly, during this activation process in MeOH the precursor CoO(OH) NPs are converted into Co(OH)₂. The implications of these results in the context of the current research in the field are also discussed.

Introduction

During the last decade, the struggle against global warming has been centered in attaining sustainable fuel generation systems. The generation of H₂ through the (photo)electrochemical reduction of protons is one of the most promising alternatives.^[1] In this context, several transition metal nanoparticles (NPs) have been shown to be catalytically active in the hydrogen evolution reaction (HER),^[2] from which cobalt, a relatively abundant 1st row transition metal, constitutes a good cheap candidate.^[3]

Co, CoO and Co(OH)₂ NPs have been successfully tested as catalysts for the HER at pH 13-14. Further, Co NPs have been encapsulated within carbon shells, carbon nanotubes (CNTs) and carbon nanofibers (CNFs) with a varied range of activities (from -196 to -375 mV overpotentials at 10 mA·cm⁻² -from now on η-) and good stability (5.5-10 h electrolysis).^[3b,3c,4] Also, mixed Co/CoO NPs have been deposited on N-doped graphitic C^[5] and Co NPs on N,S-doped C,^[6] with decreased η values of -395 and -250 mV, respectively, which remarkably further decreases to -50 mV if the Co NPs are embedded inside a CoO matrix.^[7] Finally, Co(OH)₂ NPs with variable sizes (from 1 to 30 nm) have also been successfully tested at neutral or slightly basic pH under different supports in photocatalytic hydrogen evolution.^[8,9]

In the last few years, the *in-situ* formation of catalytically active metal and metal oxide/hydroxide NPs from the decomposition of molecular precursors under catalytic conditions has been indeed described. This is very common in redox catalysis where ligands and metal centres are exposed to oxidative/reductive stress. In the case related to water oxidation, the work of Spiccia and co-workers dealing with the formation of MnO_x NPs inside a Nafion matrix from a wide set of structurally diverse Mn-based complexes under photoelectrochemical catalytic conditions is particularly revealing.^[10] The size and catalytic performance of the formed NPs is found to be highly dependent on the structure of the molecular precursor and thus on the nature of the ligands bonded to the Mn ion. For the particular case of Co ions, the *in-situ* formation of Co(OH)_x and CoO_x NPs as the real active catalytic water oxidation species when starting from mononuclear Co complexes and from a Co polyoxometalate, respectively, has also been described.^[11] Interestingly, formation of Co-derived NPs has also been observed under HER catalytic conditions at modest cathodic potentials (-0.75 V vs. NHE) in the presence of acid in acetonitrile.^[3a]

In this work, CoO and CoO(OH) NPs have been obtained by decomposition in several organic solvents of the molecular Co^I/Co^{III} complex [Co₈Na₄(L)₄(OH)₂(CO₃)₂(py)₁₀](BF₄)₂ (**1**; py = Pyridine; L = 2,6-bis-(3-oxo-3-(2-hydroxyphenyl)-propionyl)-pyridine)^[12] that are able to electrochemically form H₂ from water at pH 14. The NPs have been deposited onto the surface of a glassy carbon (GC) electrode after applying a potential of -1.86 V vs. NHE during 1 h in different solvents, and characterized by SEM, EDX, XPS and electrochemical techniques. The electrocatalytic properties of the as-deposited NPs and those of a new Co(OH)₂ phase generated under catalytic conditions have been analysed using the protocol for catalysts benchmarking recently reported by Jaramillo *et al.*^[13] The implications of these results in the context of the current research in catalytic HER by Co-derived NPs are also discussed.

a Dr. R. Bofill, Dr. X. Sala, M. Gil-Sepulcre, Dr. J. García-Antón, Prof. A. Llobet
Departament de Química, Facultat de Ciències
Universitat Autònoma de Barcelona
08193 Bellaterra, Catalonia (Spain)
E-mail: roger.bofill@uab.cat, xavier.sala@uab.cat

b M. Gil-Sepulcre, Dr. C. Gimbert-Suriñach, Prof. A. Llobet
Institut Català d'Investigació Química (ICIQ), Barcelona Institute of Science and Technology (BIST)
Av. Països Catalans 16, 43007 Tarragona, Catalonia (Spain)

c Dr. G. Aromí, Dr. D. Aguilà, Dr. V. Velasco
Departament de Química Inorgànica i Orgànica
Universitat de Barcelona
Avda. Diagonal 645, 08028 Barcelona, Catalonia (Spain)
E-mail: guillem.aromi@qi.ub.es

Supporting information for this article is given via a link at the end of the document.

Results

Electrodeposition and characterization of Co-derived NPs

Two years ago, Aromí *et al.* described that the heptadentate ligand 2,6-bis-(3-oxo-3-(2-hydroxyphenyl)-propionyl)-pyridine (H₄L) reacts with Co(II) salts in strong basic conditions, yielding in the presence of atmospheric CO₂ the mixed Co^{II}/Co^{III} complex [Co₈Na₄(L)₄(OH)₂(CO₃)₂(py)₁₀](BF₄)₂ (**1**; py=pyridine) containing two trapped carbonate anions in very close proximity.^[12] Given its unprecedented coordination features and the presence of 4 Co(II) and 4 Co(III) ions, we decided to study the potential applications of this complex in redox catalysis, specifically for the possible oxidative coupling of both trapped anions into a chemically interesting product. However, when studying its electrochemical features in acetonitrile (MeCN), two irreversible waves at -0.85 V and -1.50 V vs. NHE (-1.48 V and -2.13 V vs. Fc⁺/Fc) and an irreversible oxidative wave near 0.35 V vs. NHE (-0.28 V vs. Fc⁺/Fc) appeared, with a concomitant increase in their intensity upon performing several cyclic voltammetry (CV) cycles (Figure S1). This behaviour indicated that an irreversible chemical transformation of the electroactive species was taking place together with an increase of its available concentration at the electrode surface. This phenomenon could be related to an electrodeposition process on the surface of the GC electrode used for the measurements following the decomposition of **1** into bulk, nanoparticulated or layered Co-based materials. In fact, according to the literature, Co-based NPs able to electrochemically reduce water have already been reported to deposit at the electrode surface at modest cathodic potentials starting from a molecular Co(III) complex.^[3a] Thus, we decided to test the possible deposition of Co-based NPs active in HER catalysis after an electrolysis of our system at more negative potentials than those of the first and second irreversible waves, *i.e.*, at -1.16 V and -1.86 V vs. NHE, respectively. The optimum electrolysis time resulted to be 1 h, since no significant changes in the size of the NPs nor their electrocatalytic activity (see below) were detected at higher electrolysis times. The SEM micrographs of the surface of the GC electrodes obtained are shown in Figures S2 and S3, respectively. The presence of NPs containing heavy nuclei is clear from the back-scattered electron SEM micrographs (bright spots) in both cases, with average diameters of 65.5 ± 18.2 and 52.5 ± 15.7 nm after the treatment at -1.16 V and -1.86 V, respectively vs. NHE. Furthermore, the elemental analysis by EDX of the SEM data (Figure S4) indicated the presence of Co in both samples, thus confirming the formation of Co-based NPs under these conditions. Additionally, the formation of Co-derived NPs can be deduced from the gradual loss of colour intensity of the MeCN solution of **1** during its electrolysis at -1.86 V vs. NHE and the appearance of dispersed colloidal particles after 16 h (Figure S5). The depletion of the original complex from the solution is confirmed by the complete disappearance of the characteristic absorbance band at 218 nm of **1** after 16 h (Figure S6).

Since the NPs obtained at -1.86 V vs. NHE show smaller size and higher uniformity (lower standard deviation of the average diameter) compared to those formed at -1.16 V, we decided to focus our attention on the former conditions

to carry out our morphological and catalytic studies. It seems reasonable to expect higher catalytic activities with smaller NPs and thus with larger surface areas. Thus, an analogous procedure at -1.86 V vs. NHE was carried out in the presence of other solvents in which **1** is also soluble, namely dichloromethane (DCM) and methanol (MeOH). The SEM analyses showed the formation of smaller Co-derived NPs now, with average diameters of 37.5 ± 10.1 and 32.0 ± 9.3 nm for DCM and MeOH, respectively (Figures S7 and S8). Again, the presence of the element Co in the samples was confirmed by EDX (Figure S9). Furthermore, the ability of the octanuclear clustered complex **1** to transform into small and isolated NPs is demonstrated when analysing the results obtained under analogous conditions using CoCl₂ salt as Co precursor (Figure S10), now producing Co-derived NP aggregates of 0.28-0.45 μm in size with significant size dispersion.

In order to characterize the chemical composition of the as deposited-Co-derived NPs in MeCN, DCM and MeOH, XPS analyses were carried out (Figure 1 and Figure S11). The Co 2p XPS spectrum of the sample obtained in MeCN shows two main peaks at 780 and 796 eV accompanied by two broad satellite peaks at higher energies (786 and 802 eV), while for the samples obtained in DCM and MeOH the spectra are identical, basically showing only two main components at ca. 780.5 and 796 eV (Figure 1). The latter correspond to the Co 2p_{3/2} and Co 2p_{1/2} components, respectively,^[14] while the satellite peaks indicate the presence of unpaired electrons in the sample, *i.e.*, of Co^{II} (d⁷) atoms.^[15] The O 1s XPS spectra, show a single band at 530.5 eV for the MeCN sample, which is shifted towards 531.4 eV for the DCM and MeOH cases (Figure S11a). This shift towards higher energies is due to the presence of hydroxyl groups on the Co surface.^[2,7,14,16] Thus, when taking all XPS data in consideration, it is clear that in MeCN we obtain CoO NPs. This is supported by the similarity of our Co 2p XPS spectrum with those of CoO previously reported^[15] and by the presence of a band at ca. 530 eV for the O 1s XPS spectrum, as reported elsewhere.^[7,14] In sharp contrast, in DCM and MeOH mixed oxy-hydroxide Co^{III} (d⁶) NPs are obtained (CoO(OH) NPs) based on the almost complete absence of Co 2p satellite bands and the 780.5 eV value for the Co 2p_{3/2} transition^[17] as well as on the high energy shift of the O 1s band. The presence of CoO(OH) in the sample formed in DCM could be due to hydration processes provoked by air exposure prior to the XPS measurements. Regarding N and C XPS signals (Figure S11b-c), the N 1s band found ca. 399 eV for all samples is typical of Co-N bonds or N-pyridyls,^[4a-b,6] which originate from ligand L in precursor **1** during its electrodecomposition (a comparison of the N atomic percentage measured by XPS indicates that the amount of N of the samples is comprised between 8 and 15 % and thus is not negligible compared to the 0.7 % atomic percentage of the blank), and the C 1s band at ca. 284.2 eV is due to the GC electrode.^[18] From now on in this work and for the sake of brevity, the three sets of NPs formed after 1h-electrolysis at -1.86 V vs. NHE will be named as CoO-MeCN, CoO(OH)-MeOH and CoO(OH)-DCM.

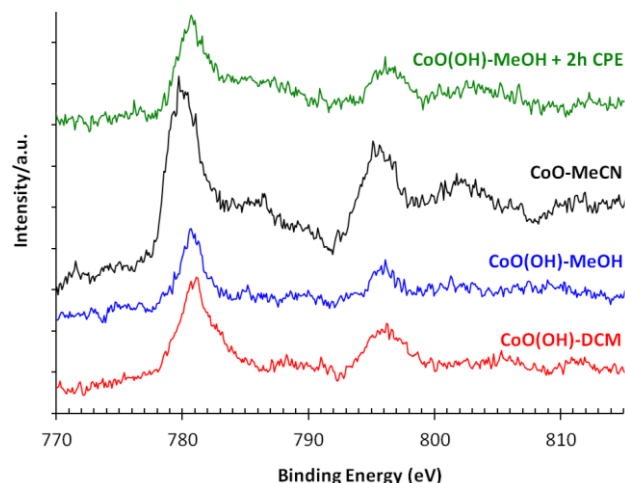


Figure 1. Co 2p XPS spectra for the Co-based NPs obtained from **1** in MeCN (black), DCM (red) and MeOH (blue) after a 1h-electrolysis at -1.86 V vs. NHE and from **1** in MeOH after a 1h-electrolysis at -1.86 V vs. NHE plus a 2h-CPE at 10 mA·cm⁻² (green). Energies have been calibrated according to the C 1s band of graphite at 284.2 eV.

Electrocatalytic performance

The Co-derived NPs deposited on the surface of a rotating disk electrode (RDE) obtained in the three different solvents were characterized by rotating disk voltammetry (RDV) at pH 14 (Figure 2), where an intense irreversible catalytic current with onset potential at ca. -1.11, -1.15 and -1.20 V vs. NHE appears for CoO-MeCN, CoO(OH)-MeOH and CoO(OH)-DCM, respectively, with associated current densities of 1.27, 0.76 and 0.26 mA/cm². According to H₂-sensitive Clark electrode measurements, this process corresponds to the reduction of protons to generate H₂ with a faradaic efficiency between 96% and 98% for all cases (Figure S12). From the experimental onset potential of the catalytic waves compared to the thermodynamic reduction potential $E(\text{H}^+/\text{H}_2)$ at pH 14 (-0.828 V vs. NHE), the MeCN, MeOH and DCM samples show an onset overpotential of -276 mV, -321 mV and -348 mV, respectively.

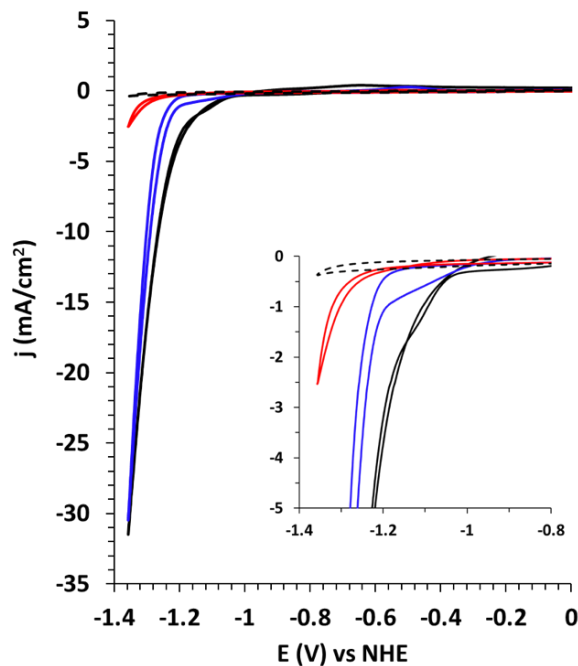


Figure 2. Representative rotating disk voltammograms of CoO(OH)-DCM (red), CoO(OH)-MeOH (blue) and CoO-MeCN (black). The non-functionalized RDE electrode (blank) is shown as a black dashed line. Conditions: N₂-Saturated 1 M NaOH solution, 0.01 V/s scan rate and 1600 rpm. Inset: zoomed view of the onset potential region.

A thorough electrochemical analysis of the behaviour of the Co-based NPs has been performed following the procedures described by Jaramillo *et al.*^[13] Thus, the electrochemically active surface area (ECSA) of each modified RDE with Co-based NPs was estimated from its electrochemical double-layer capacitance (C_{dl}) by measuring the non-Faradaic capacitive current associated with double-layer charging (Figure S13). The roughness factor (RF) is calculated by dividing the estimated ECSA by the geometric area of the electrode. Furthermore, 30s-controlled current step-chronopotentiometry and chronoamperometry (Fig. S14) and 2h-controlled current electrolysis (Figure 3a and Fig. S15) measurements have allowed us to determine the overpotential at a constant current density of 10 mA·cm⁻² (η). This is a widely accepted benchmarking parameter for the catalytic activity of heterogeneous catalysts which corresponds to the approximate current density expected for a 10% efficient solar-to-fuel conversion photoelectrochemical cell under 1 sun illumination^[19] (Figure S14). The NPs with lower η are CoO-MeCN (-435 mV), followed by CoO(OH)-MeOH (-465 mV) and finally by CoO(OH)-DCM (-504 mV). Interestingly, when the CoO-MeCN and CoO(OH)-DCM NPs are submitted to a 2h-controlled current electrolysis at a constant current density of 10 mA·cm⁻² (Figure S15), the η steadily increases, particularly for CoO-MeCN, denoting the relative instability of both systems under HER conditions. Effectively, XPS (Fig S16) and SEM analyses (Fig. S17 and S18) show the lack of stability of both CoO-MeCN and CoO(OH)-DCM NPs after a 2h-controlled current electrolysis. For the former case, no Co-derived NPs are detected on the surface of the GC electrode, and for the latter the CoO(OH) composition of the NPs is maintained, although their

concentration clearly decreases (less intense Co 2p signal and decrease of the Co atomic concentration from 1.61 % to 0.64 % according to XPS measurements, Fig. S16) while at the same time the average diameter increases from 37.5 nm (Figure S7) to 77.7 nm (Figure S18).

In contrast, as shown in Figure 3a, the η of CoO(OH)-MeOH NPs clearly decreases over time. The superior activity of the resulting nanomaterial after electrolysis is also appreciated when comparing its RDV with that of the original CoO(OH) NPs in the same conditions (Figure 3b). A detailed electrocatalytic analysis of this "activated" system can be found in Figures S19-S21 of the Supplementary Material. The results corroborate its higher performance, with a decrease in η by 213 mV and a significant increase in the specific current density (j_s) at an overpotential of -480 mV, which is more than triplicated, from 174 to 596 mA·cm⁻².

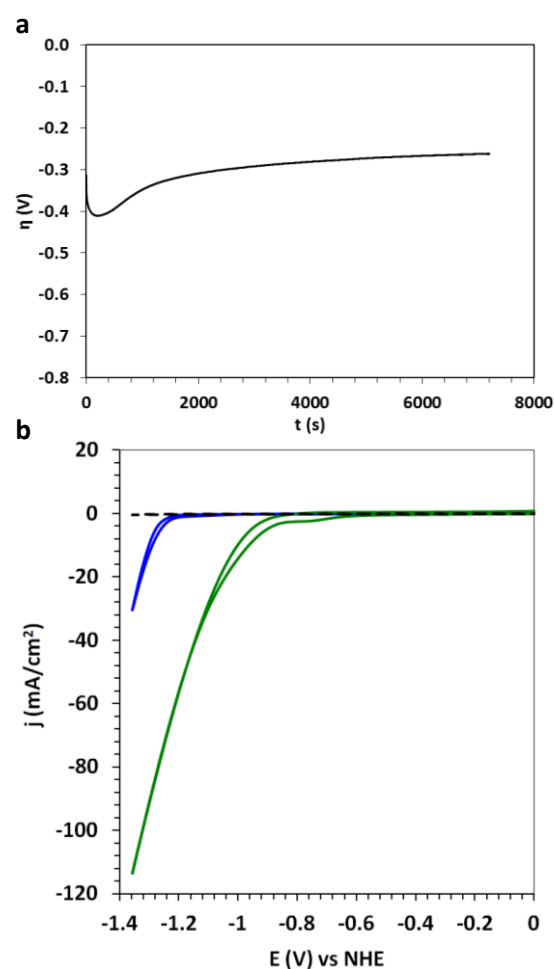


Figure 3. a) 2h-controlled current electrolysis in MeOH at 10 mA·cm⁻² of CoO(OH)-MeOH; b) representative rotating disk voltammograms of CoO(OH)-MeOH at $t=0$ (blue) and after a 2h-controlled current electrolysis at 10 mA·cm⁻² (green). The non-functionalized RDE electrode (blank) is shown as a dashed line. Conditions: N₂-Saturated 1 M NaOH solution, 0.01 V/s scan rate and 1600 rpm.

In order to better understand the nature of this "activated" system, the 2h-electrolyzed cathode was characterized by SEM (Fig. S22 and S23) and XPS (Figure 1

and Figure S11). SEM images show an average diameter of 39.9 ± 16.4 nm, very close to the precursor CoO(OH) NPs before the activation (Figure S8).

Comparison of the Co 2p XPS spectra of the CoO(OH)-MeOH sample and its 2h-electrolyzed derivative shows the appearance of two satellite bands for the latter (Figure 1) and the presence of an O 1s XPS band at 531.2 eV in both samples (Figure S11a). Thus, a reduction of the Co^{III} atoms to Co^{II} is taking place without losing hydroxyl groups. Therefore, we propose the formation of Co(OH)₂ NPs after the 2h activation process in MeOH. Indeed, the positions of the Co 2p main peaks at 780.7 and 796.5 eV as well as the overall shape of the spectrum are coincident with previous data reported for Co(OH)₂.^[8,11a,15,17] Curiously, the low intensity shoulder at ca. 287.5 eV of its C 1s XPS spectrum (Figure S11c) could be attributed to the presence of MeOH molecules coordinated onto the surface of the Co(OH)₂ NPs.^[20]

Finally, the Tafel plots for all four Co-derived NPs and two blanks prepared in MeOH from CoCl₂ and CoCl₂ in the presence of H₄L are shown in Figure 4, in which it becomes clear the superior HER activity of the Co(OH)₂ NPs obtained after a 2h-CPE in MeOH (red line).

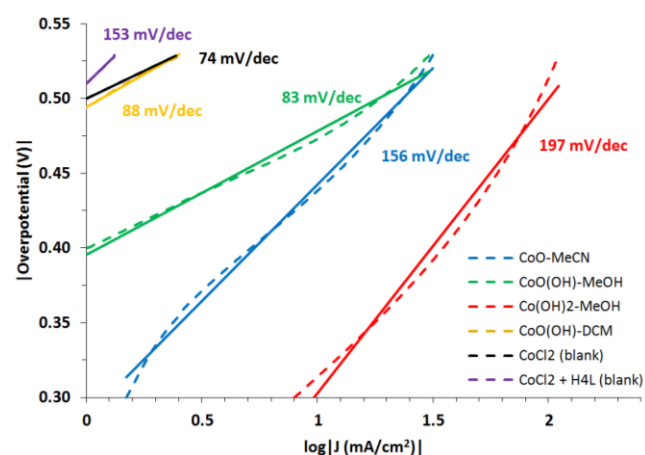


Figure 4. Tafel plots registered at pH 14 for the Co-based NPs synthesized in this work in different solvents and from CoCl₂ or CoCl₂ + H₄L in MeOH (blanks).

Discussion

A comparison of the physical and electrochemical properties of the Co-derived NPs formed from **1** in this work with those of the respective blanks prepared from CoCl₂ is shown in Table 1. In all cases, the NPs obtained in the blanks (entries 5-8) are one order of magnitude larger and less uniformly sized than their respective NPs formed from **1** (entries 1-3), showing the relevant role of the molecular precursor for its proper reduction into small Co-derived NPs. This result highlights the already reported role of metal complexes in allowing better control over *in-situ* electrodeposition processes than simple salts.^[10b] Thus, the initial η ($\eta_{t=0}$) and the η value after 2h-electrolysis ($\eta_{t=2}$) are normally higher than the respective values for the NPs obtained from **1** (entries 1 vs. 5, 2 vs. 6 and 3 vs. 7) while the j_s values are between 1 and 3 orders of magnitude lower. Also, the presence of

uncoordinated H₄L ligand in the CoCl₂ blank prepared in MeOH does not significantly alter the performance of the obtained NPs compared to the blank prepared in its absence

(entries 7 and 8), thus pointing to the importance of starting from a precursor containing the ligand within its molecular scaffold.

Table 1. Physical and electrochemical properties of the Co-derived NPs synthesized in this work onto the surface of a RDE electrode.

Entry	Co Precursor	Solvent	NP ^[a]	diameter (nm) ^[b]	ECSA ^[c]	RF ^[c]	Onset η (mV) ^[d]	$\eta_{t=0}$ (mV) ^[e]	$\eta_{t=2}$ (mV) ^[f]	j_s @ $\eta=-480$ mV (mA·cm ⁻²) ^[g]	ε ^[h]
1	1	MeCN	CoO	52.5 ± 15.7	0.14 ± 0.02	1.14 ± 0.19	-276 ± 47	-435 ± 29	-669 ± 37	225 ± 30	96%
2	1	DCM	CoO(OH)	37.5 ± 10.1	0.08 ± 0.01	0.65 ± 0.11	-348 ± 28	-504 ± 20	-595 ± 12	20 ± 10	98%
3	1	MeOH	CoO(OH)	32.0 ± 9.3	0.15 ± 0.02	1.24 ± 0.18	-321 ± 78	-465 ± 98	-252 ± 16	174 ± 124	98%
4	CoO(OH)	MeOH	Co(OH) ₂ ^[i]	39.9 ± 16.4	0.15 ± 0.02	1.24 ± 0.18	-140 ± 74	-246 ± 20	n.d.	596 ± 216	98%
5	CoCl ₂	MeCN	n.d. ^[j]	448 ± 146	0.14 ± 0.04	1.21 ± 0.06	-367 ± 80	-461 ± 97	n.d.	0.46 ± 0.28	n.d.
6	CoCl ₂	DCM	n.d.	325 ± 280	0.08 ± 0.01	0.64 ± 0.09	-390 ± 60	-475 ± 70	n.d.	0.56 ± 0.31	n.d.
7	CoCl ₂	MeOH	n.d.	283 ± 175	0.13 ± 0.02	1.07 ± 0.19	-398 ± 15	-515 ± 88	-679 ± 70	15 ± 14	n.d.
8	CoCl ₂ + H ₄ L	MeOH	n.d.	n.d.	0.16 ± 0.02	1.24 ± 0.20	-406 ± 45	-544 ± 30	-572 ± 20	11 ± 8	n.d.

[a] Formed during 1h-electrolysis at -1.86 V vs. NHE at 1600 rpm and determined by XPS analyses. [b] Determined by SEM analyses. [c] Electrochemically-active surface area (ECSA) and roughness factor (RF) determined according to Jaramillo *et al.*^[13] The double-layer capacitance of the systems has been calculated as the average of the absolute value of the slopes of their linear fits to the data shown in Figures S13 and S19. [d] Onset overpotential of the electrocatalytic wave estimated from RDV experiments. [e] Overpotential required for reaching a 10 mA·cm⁻² current density. The values have been estimated from the 30 s step-chronopotentiometry and chronopotentiometry experiments. [f] Overpotential required for reaching 10 mA·cm⁻² current density after a 2h-controlled current electrolysis experiment. [g] Specific current density (j_s) obtained by dividing the experimental current density (j , in mA·cm⁻²) by the ECSA at an overpotential of -480 mV. [h] ε = Faradaic efficiency. [i] The precursor are the CoO(OH) NPs obtained in MeOH after 1h-electrolysis of **1** at -1.86 V vs. NHE, which are then submitted to a 2h-CPE experiment at 10 mA·cm⁻². [j] n.d. = not determined.

The ECSA and RF values of our Co-based NPs are similar, assuming the one order of magnitude inherent accuracy of the RF measurements, while they are significantly lower -around three orders of magnitude- than those of Co electrodes previously benchmarked.^[13] These results are consistent with the fact that in our case low concentrations of **1** are used for the NP electrodeposition (0.25 mM) compared to the much higher concentrations used in the literature (around 100 mM).^[13] The low ECSA values combined with the high catalytic currents measured translate into particularly high specific current densities (j_s) in the HER when measured at an overpotential of -480 mV (entries 1-4, Table 1).

On the other hand, the CoO-MeCN and CoO(OH)-DCM NPs suffer from an increase in η over time (entries 1 and 2), specially in the former case. This decrease in the HER activity is more pronounced than that previously reported for the best metallic cathodes by Jaramillo *et al.*^[13] Furthermore, the XPS and SEM measurements performed after a 2h-CPE (Figs. S16-S18) have shown the instability of these nanoparticulated systems, probably due to the inability of MeCN and DCM to form stabilizing hydrogen bonds with the NPs (see below). However, despite this drawback, our Faradaic efficiencies are comprised in the 96-98% range, which stand out among the normal values found for some of the best metal-based HER catalysts reported so far at pH 14.^[13]

Contrastingly, CoO(OH)-MeOH NPs undergo a dramatic decrease in η over time while being converted into Co(OH)₂ NPs (entries 3 and 4), reaching a $\eta_{t=2}$ value as low as ca. -250 mV at pH 14. This overpotential is lower than that of other published Co-based NP systems under analogous conditions. Thus, Co NPs encapsulated in N-rich CNTs have shown an η of -375 mV at pH 14,^[3b] whereas Co/CoO^[5] and Co NPs^[4a] immobilized on N-doped and Co-N-doped C feature η values of -395 and -314 mV, respectively, at pH 13. Also, a similar η of -250 mV has been measured at pH 14 for Co NPs on N,S-doped C^[6] and for trimetallic CoNiFe NPs.^[13] Additional data on additional recently published Co-derived nanosystems applied in electrochemical HER catalysis can be found in Table S1.

Concerning the CoO(OH)-DCM NPs, it is difficult to rationalize why, having very similar size and RF values as those of CoO(OH)-MeOH (entries 2 and 3), they clearly possess lower HER catalytic activity and stability (*i.e.*, higher η -specially over time- and one order lower j_s value, and even higher $\eta_{t=0}$ than its CoCl₂ blank counterpart). This may be due in part to slower mass transport of H⁺ into the NPs in the case of DCM, as suggested by Jaramillo *et al.* during the catalytic performance of metallic nanoporous films compared to non-nanoporous films made from the same metal.^[13] Thus, the CoO(OH) NPs obtained in DCM may have a different structure than those synthesized in MeOH, probably because of the non-coordinating and non-hydrogen bonding ability of

1 DCM, which may lead to less stable NPs. In fact, previous
2 studies with metallic NPs have demonstrated their
3 morphology dependence with the nature/polarity of the
4 solvent employed for their synthesis.^[21] Furthermore, it is
5 likely that the hydrogen binding abilities of MeOH -completely
6 absent in DCM and MeCN- may play a key role in the
7 stabilization of CoO(OH) NPs and their further conversion into
8 the more active Co(OH)₂ NPs during the 2h-CPE.
9 Contrastingly, the non-hydrogen binding abilities of both DCM
10 and MeCN may be one of the reasons for the progressive
11 deactivation of the CoO(OH)-DCM and CoO-MeCN NPs
12 along time. Nonetheless, the amount of N and C coming from
13 the ligand initially present in **1** or fragments of it within all Co-
14 derived NPs (see N 1s and C 1s XPS data of Figure S11b-c
15 of the Supplementary Material) should not be ignored, since
16 these elements may not only contribute to the formation of
17 small and highly dispersed NPs but could also provide a
18 stabilizing effect to the NPs during catalysis. However, an
19 exact determination of the amount of C and N originating from
20 **1** is not possible given the use of GC electrodes as supports
21 and the presence of N in the supporting electrolyte (TBAPF₆)
22 and in MeCN.

23 Finally, from the analysis of the Tafel plots (Figure 4) it
24 also becomes obvious that the three more active systems
25 (the ones on the right hand side of the graph) are those
26 obtained from **1** in MeCN and MeOH (in fact, the activity of
27 CoO(OH)-DCM is very close to that of the CoCl₂ blank
28 obtained in MeOH). The slopes for CoO-MeCN, CoO(OH)-
29 MeOH and Co(OH)₂ are close or above 100 mV/dec.
30 Therefore, consistent with the literature,^[22] the rate
31 determining step (rds) for the HER reaction in our three most
32 active systems must be the Volmer step, i.e., the
33 electrochemical H adsorption onto the NP surface. On the
34 other hand, the crossing of the CoO-MeCN (blue line) and the
35 CoO(OH)-MeOH (green line) curves confirms that the former
36 is more active (higher *j*) at an overpotential lower than ca. -
37 520 mV, but that at overpotentials more negative than -520
38 mV the latter performs better in HER.

39 Conclusions

40
41
42
43 In this work, we have demonstrated that the molecular
44 Co^I/Co^{III} complex **1** generates electrodeposited ~50 nm CoO
45 or ~35 nm CoO(OH) NPs depending on the solvent employed
46 (MeCN for the former, MeOH or DCM for the latter) from its
47 decomposition at -1.86 V vs. NHE. The resulting cathodes,
48 possessing low and comparable ECSA and RF values,
49 catalyze the electrochemical reduction of water at pH 14 with
50 distinctive specific activities (*j_s*) under the application of a -480
51 mV bias. The most active system at t=0 h is CoO-MeCN
52 ($\eta_{t=0}=-435$ mV, $j_s=225$ mA·cm⁻² at an overpotential of -480
53 mV). However, the CoO(OH)-MeOH NPs, with an initial
54 catalytic activity very close to those of CoO-MeCN, become
55 significantly more active after a 2h constant polarization
56 process at 10 mA·cm⁻² ($\eta_{t=2}=-250$ mV, $j_s=596$ mA·cm⁻² at an
57 overpotential of -480 mV). These activated NPs correspond to
58 Co(OH)₂ according to XPS analysis, which show better HER
59 performance than many Co-based NP systems published
60 elsewhere under analogous conditions. Contrastingly, the
61 HER activity steadily decreases for CoO-MeCN and
62

63
64
65
66
67
68
69
70
71
72
73
74
75
76
77
78
79
80
81
82
83
84
85
86
87
88
89
90
91
92
93
94
95
96
97
98
99
100
101
102
103
104
105
106
107
108
109
110
111
112
113
114
115
116
117
118
119
120
121
122
123
124
125
126
127
128
129
130
131
132
133
134
135
136
137
138
139
140
141
142
143
144
145
146
147
148
149
150
151
152
153
154
155
156
157
158
159
160
161
162
163
164
165
166
167
168
169
170
171
172
173
174
175
176
177
178
179
180
181
182
183
184
185
186
187
188
189
190
191
192
193
194
195
196
197
198
199
200
201
202
203
204
205
206
207
208
209
210
211
212
213
214
215
216
217
218
219
220
221
222
223
224
225
226
227
228
229
230
231
232
233
234
235
236
237
238
239
240
241
242
243
244
245
246
247
248
249
250
251
252
253
254
255
256
257
258
259
260
261
262
263
264
265
266
267
268
269
270
271
272
273
274
275
276
277
278
279
280
281
282
283
284
285
286
287
288
289
290
291
292
293
294
295
296
297
298
299
300
301
302
303
304
305
306
307
308
309
310
311
312
313
314
315
316
317
318
319
320
321
322
323
324
325
326
327
328
329
330
331
332
333
334
335
336
337
338
339
340
341
342
343
344
345
346
347
348
349
350
351
352
353
354
355
356
357
358
359
360
361
362
363
364
365
366
367
368
369
370
371
372
373
374
375
376
377
378
379
380
381
382
383
384
385
386
387
388
389
390
391
392
393
394
395
396
397
398
399
400
401
402
403
404
405
406
407
408
409
410
411
412
413
414
415
416
417
418
419
420
421
422
423
424
425
426
427
428
429
430
431
432
433
434
435
436
437
438
439
440
441
442
443
444
445
446
447
448
449
450
451
452
453
454
455
456
457
458
459
460
461
462
463
464
465
466
467
468
469
470
471
472
473
474
475
476
477
478
479
480
481
482
483
484
485
486
487
488
489
490
491
492
493
494
495
496
497
498
499
500
501
502
503
504
505
506
507
508
509
510
511
512
513
514
515
516
517
518
519
520
521
522
523
524
525
526
527
528
529
530
531
532
533
534
535
536
537
538
539
540
541
542
543
544
545
546
547
548
549
550
551
552
553
554
555
556
557
558
559
560
561
562
563
564
565
566
567
568
569
570
571
572
573
574
575
576
577
578
579
580
581
582
583
584
585
586
587
588
589
590
591
592
593
594
595
596
597
598
599
600
601
602
603
604
605
606
607
608
609
610
611
612
613
614
615
616
617
618
619
620
621
622
623
624
625
626
627
628
629
630
631
632
633
634
635
636
637
638
639
640
641
642
643
644
645
646
647
648
649
650
651
652
653
654
655
656
657
658
659
660
661
662
663
664
665
666
667
668
669
670
671
672
673
674
675
676
677
678
679
680
681
682
683
684
685
686
687
688
689
690
691
692
693
694
695
696
697
698
699
700
701
702
703
704
705
706
707
708
709
710
711
712
713
714
715
716
717
718
719
720
721
722
723
724
725
726
727
728
729
730
731
732
733
734
735
736
737
738
739
740
741
742
743
744
745
746
747
748
749
750
751
752
753
754
755
756
757
758
759
760
761
762
763
764
765
766
767
768
769
770
771
772
773
774
775
776
777
778
779
780
781
782
783
784
785
786
787
788
789
790
791
792
793
794
795
796
797
798
799
800
801
802
803
804
805
806
807
808
809
810
811
812
813
814
815
816
817
818
819
820
821
822
823
824
825
826
827
828
829
830
831
832
833
834
835
836
837
838
839
840
841
842
843
844
845
846
847
848
849
850
851
852
853
854
855
856
857
858
859
860
861
862
863
864
865
866
867
868
869
870
871
872
873
874
875
876
877
878
879
880
881
882
883
884
885
886
887
888
889
890
891
892
893
894
895
896
897
898
899
900
901
902
903
904
905
906
907
908
909
910
911
912
913
914
915
916
917
918
919
920
921
922
923
924
925
926
927
928
929
930
931
932
933
934
935
936
937
938
939
940
941
942
943
944
945
946
947
948
949
950
951
952
953
954
955
956
957
958
959
960
961
962
963
964
965
966
967
968
969
970
971
972
973
974
975
976
977
978
979
980
981
982
983
984
985
986
987
988
989
990
991
992
993
994
995
996
997
998
999
1000

Experimental Section

All reagents used in the present work were obtained from Sigma Aldrich in reagent grade and were used without further purification. Reagent grade organic solvents were obtained from Scharlab and Panreac. Anhydrous CoCl₂ was supplied by Sigma Aldrich. NaOH was obtained from Panreac (99%), and milliQ quality grade water was employed. [Co₈Na₄(L)₄(OH)₂(CO₃)₂(py)₁₀](BF₄)₂ (**1**) was prepared as previously reported.^[12]

UV-Vis spectroscopy was performed on a HP8453 spectrometer using 1 cm quartz cells. Scanning Electron Microscopy (SEM) and Energy-dispersive X-Ray Spectroscopy (EDX) analyses were performed using a JEOL JSM 6700F electron microscope working at 10 kV.

X-ray photoelectron spectroscopy (XPS) experiments were performed with a SPECS EA10P hemispherical analyser using a non-monochromated X-ray source (Al K α line of 1486.6 eV and 300W). The direction of the X-ray source with respect to the sample was 90° and ultrahigh vacuum was maintained during the measurements, obtaining a residual pressure of 10⁻⁸ Pa. GC electrodes analysed by SEM and XPS were functionalized for 1h by applying a constant potential (-1.86 V or -1.16 V vs. NHE) to a solution of **1** (0.6 mg, 2 μ mol) in the different solvents assayed. Afterwards, the GC surface was washed with distilled H₂O, MeCN and acetone. Then, a small section of the electrode was cut on a Mintom rotating saw (Struers) equipped with a metal cut-off wheel, washed again with distilled H₂O, acetone and Et₂O and dried over vacuum for 2h.

Electrochemical measurements were carried out on a Bio Logic Science Instrument SP-150 potentiostat and CHI660D potentiostat using a three-electrode cell. A glassy carbon (GC, 3 mm internal diameter) or a rotating disk electrode (RDE, 4 mm GC disk diameter) were employed as working electrodes, while a platinum wire was used as counter electrode and Hg/HgSO₄ or SCE were used as the reference electrodes. The solvents used for functionalization of the electrode (acetonitrile, methanol or dichloromethane) were prepared containing the necessary amount of n-Bu₄NPF₆ (TBAPF₆) as supporting electrolyte to yield a 0.1 M ionic strength. Electrodeposition of Co NPs was carried out in a 10 mL three electrode cell using RDE as working electrode, platinum as counter electrode and Hg/HgSO₄ as reference electrode. Before each functionalization, the RDE electrode was polished with 1 and 0.05 micron alumina suspension in distilled water, sonicated for 5 min in H₂O and

1 washed with distilled water and acetone before each
2 measurement. 1 mg (0.3 μmol) of **1** was sonicated in the 10
3 mL three electrode cell until complete solution in 3 mL of the
4 corresponding organic solvent (MeCN, DCM or MeOH)
5 containing 0.1 M of electrolyte (TBAPF₆). Subsequently, a
6 constant potential of -1.86 V or -1.16 V vs. NHE was applied
7 to the solution for 1 hour. Finally, the functionalized RDE
8 electrode was washed with distilled H₂O, MeCN and acetone
9 and dried over vacuum for 30 minutes before electrochemical
10 measurements.

11 For the electrochemical characterization and catalytic
12 experiments in HER, the cell was purged for 30 minutes with
13 N₂ and was continuously bubbled during the measurements.
14 The resistance of the cell (typically R_u ~ 13 Ω) was
15 compensated at 85%. In the case of electrochemical
16 capacitance measurements, linear sweep voltammetry (LSV)
17 was performed in a potential window where there is a non-
18 Faradaic current response as determined from cyclic
19 voltammetry. This range is typically 0.1 V centred on the
20 Open-circuit potential (OCP) for each electrode. The
21 measurements were carried out by sweeping the potential
22 across the selected potential range at 8 different scan rates
23 (0.005, 0.01, 0.025, 0.05, 0.1, 0.2, 0.4, 0.8 V/s). The working
24 electrode was held at the starting potential before beginning
25 the next LSV experiment.

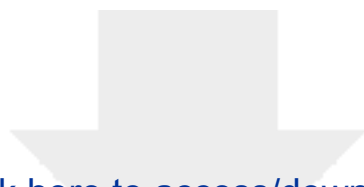
26 For Faradaic efficiency measurements, H₂ was
27 quantified using a Unisense H₂-probe controlled by a
28 Unisense Microprocessor Multimeter. Measurements were
29 carried out in a U-compartment cell containing a
30 functionalized GC electrode (3 mm diameter), a reference
31 electrode (Ag/AgCl) and the hydrogen probe in the first
32 compartment and a counter electrode in the second
33 compartment, both separated by a frit and filled with 15 mL of
34 NaOH solution (pH 14). For H₂ measurements, the solution
35 was degassed with a N₂ flow for 30 minutes under vigorous
36 stirring. The baseline was recorded for 20 minutes and a
37 constant potential of -1.86 V vs. NHE was held at the working
38 electrode containing Co NPs for 30 min. The increase in
39 pressure of H₂ was monitored during this time, and from this
40 the total amount of H₂ gas formed was determined. Finally,
41 Faradaic efficiency was calculated by dividing the total
42 amount of H₂ produced during the experiment by the
43 theoretical amount calculated from the total charge passed in
44 the bulk-electrolysis experiment.

45 Acknowledgements

46 Support from MINECO/FEDER (CTQ2015-64261-R and
47 CTQ2016-80058-R) is gratefully acknowledged. M. G.-S. is
48 grateful for the award of a PIF doctoral grant from UAB. J. G.-
49 A. acknowledges the Serra Hünter Program. G. A., D. A. and
50 V. V. thank the ERC for contracts under ERC Starting Grant
51 StG-2010-258060 and the Generalitat de Catalunya for the
52 prize ICREA Academia 2008 and 2013. We also thank the
53 Servei de Microscopia Electrònica, Universitat Autònoma de
54 Barcelona, for allocating instrument time.

55 **Keywords:** CoOx • Electrocatalysis • H₂ evolution • transition
56 metal chemistry
57
58

- 59
60
61
62
63
64
65
- [1] a) Z. Han, R. Eisenberg, *Acc. Chem. Res.* **2014**, *47*, 2537-2544; b) M. Wang, K. Han, S. Zhang, L. Sun, *Coord. Chem. Rev.* **2015**, *287*, 1-14; c) Y. Xu, B. Zhang, *Cat. Sci. & Tech.* **2015**, *5*, 3084-3096; d) N. Jiang, B. You, M. Sheng, Y. Sun, *Angew., Chem. Int. Ed.* **2015**, *54*, 6251-6254; e) B. You, N. Jiang, M. Sheng, M. W. Bhushan, Y. Sun, *ACS Catal.* **2016**, *6*, 714-721; f) B. You, X. Liu, X. Liu, Y. Sun, *ACS Catal.* **2017**, *7*, 4564-4570; g) B. You, Y. Sun, *Adv. Energy Mater.* **2016**, *6*, 1502333.
- [2] S. Fukuzumi, Y. Yamada, *J. Mater. Chem.* **2012**, *22*, 24284-24296.
- [3] a) E. Anxolabéhère-Mallart, C. Costentin, M. Fournier, S. Nowak, M. Robert, J.-M. Savéant, *J. Am. Chem. Soc.* **2012**, *134*, 6104-6107; b) X. Zou, X. Huang, A. Goswami, R. Silva, B. R. Sathe, E. Mikmekov, T. Asefa, *Angew. Chem., Int. Ed.* **2014**, *53*, 4372-4376; c) E. Zhang, Y. Xie, S. Ci, J. Jia, P. Cai, L. Yia, Z. Wen, *J. Mat. Chem. A* **2016**, *4*, 17288-17298.
- [4] a) Y. Wang, Y. Nie, W. Ding, S. G. Chen, K. Xiong, X. Q. Qi, Y. Zhang, J. Wang, Z. D. Wei, *ChemComm.* **2015**, *51*, 8942-8945; b) H. Su, H.-H. Wang, B. Zhang, K.-X. Wang, X.-H. Lin, J.-S. Chenn, *Nano Energy* **2016**, *22*, 79-86.
- [5] X. Zhang, R. Liu, Y. Zang, G. Liu, G. Wang, Y. Zhang, H. Zhang, H. Zhao, *ChemComm.* **2016**, *52*, 5946-5949.
- [6] W. Deng, H. Jiang, C. Chen, L. Yang, Y. Zhang, S. Peng, S. Wang, Y. Tan, M. Ma, Q. Xie, *ACS Appl. Mater. Interfaces* **2016**, *8*, 13341-13347.
- [7] X. Liu, C. Dong, W. Dong, X. Wang, X. Yuan, F. Huang, *RSC Adv.* **2016**, *6*, 38515-38520.
- [8] Z. Li, Y. Wu, G. Lu, *Appl. Cat. B: Environm.* **2016**, *188*, 56-64.
- [9] a) H. Dang, X. Dong, Y. Dong, H. Fan, Y. Qiu, *Mater. Lett.* **2015**, *138*, 56-59; b) H. Wender, R. V. Gonçalves, C. S. B. Dias, M. J. M. Zapata, L. F. Zagonel, E. C. Mendonça, S. R. Teixeira, F. Garcia, *Nanoscale* **2013**, *5*, 9310-9316.
- [10] a) R. K. Hocking, R. Brimblecombe, L.-Y. Chang, A. Singh, M. H. Cheah, C. Glover, W. H. Casey, L. Spiccia, *Nat. Chem.* **2011**, *3*, 461-466; b) A. Singh, R. K. Hocking, S. L.-Y. Chang, B. M. George, M. Fehr, K. Lips, A. Schnegg, L. Spiccia, *Chem. Mater.* **2013**, *25*, 1098-1108.
- [11] a) D. Hong, J. Jung, J. Park, Y. Yamada, T. Suenobu, Y.-M. Lee, W. Nam, S. Fukuzumi, *Energy Environ. Sci.* **2012**, *5*, 7606-7616; b) J. J. Stracke, R. G. Finke, *J. Am. Chem. Soc.* **2011**, *133*, 14872-14875.
- [12] V. Velasco, D. Aguilà, L. A. Barrios, I. Borilovic, O. Roubeau, J. Ribas-Ariño, M. Fumanal, S. J. Teat, G. Aromí, *Chem. Sci.* **2015**, *6*, 123-131.
- [13] C. C. L. McCrory, S. Jung, I. M. Ferrer, S. M. Chatman, J. C. Peters, T. F. Jaramillo, *J. Am. Chem. Soc.* **2015**, *137*, 4347-4357.
- [14] A. Indra, P. W. Menezes, C. Das, C. Göbel, M. Tallarida, D. Schmeißer, M. Driess, *J. Mat. Chem. A* **2017**, *5*, 5171-5177.
- [15] M. C. Biesinger, B. P. Payne, A. P. Grosvenor, L. W. M. Lau, A. R. Gerson, R. St. C. Smart, *Appl. Surf. Sci.* **2011**, *257*, 2717-2730.
- [16] J. Fester, M. García-Melchor, A. S. Walton, M. Bajdich, Z. Li, L. Lammich, A. Vojvodic, J. V. Lauritsen, *Nat. Commun.* **2017**, *8*, 14169, 1-8.
- [17] J. Yang, H. Lu, W. N. Martens, R. L. Frost, *J. Phys. Chem. C* **2010**, *114*, 111-119.
- [18] a) L. J. Fang, X. L. Wang, Y. H. Li, P. F. Liu, Y. L. Wang, H. D. Zeng, H. G. Yang, *Appl. Catal B: Environ.* **2017**, *200*, 578-584; b) X. Yue, S. Yi, R. Wang, Z. Zhang, S. Qiu, *Nat. Sci. Reports* **2017**, *6*:22268, 1-8.
- [19] M. G. Walter, E. L. Warren, J. R. McKone, S. W. Boettcher, Q. Mi, E. A. Santori, N. S. Lewis, *Chem. Rev.* **2010**, *110*, 6446-6473.
- [20] A. K. Agegnehu, C.-J. Pan, J. Rick, J.-F. Lee, W.-N. Su, B.-J. Hwang, *J. Mater. Chem.* **2012**, *22*, 13849-13854.
- [21] K. Pelzer, O. Vidoni, K. Philippot, B. Chaudret, V. Collière, *Adv. Funct. Mater.* **2003**, *13*, 118-126.
- [22] Y. Zheng, Y. Jiao, M. Jaroniec, S. Z. Qiao, *Angew. Chem., Int. Ed.* **2015**, *54*, 52-65.



Click here to access/download

Supporting Information

ESI_Catalytic H₂ evolution with Co NPs_EJIC.pdf

